Tomographic evidence for a slab tear induced by fossil ridge subduction at Manila Trench, South China Sea

Article *in* International Geology Review · December 2014

DOI: 10.1080/00206814.2014.929054

CITATIONS
4

READS
169

3 authors, including:

Jianke Fan
Chinese Academy of Sciences
2 PUBLICATIONS **4** CITATIONS

SEE PROFILE

International Geology Review
Publication details, including instructions for authors and subscription information:
http://www.tandfonline.com/loi/tigr20

Tomographic evidence for a slab tear induced by fossil ridge subduction at Manila Trench, South China Sea

Jian-ke Fan[ab], Shi-guo Wu[ab] & George Spence[c]
[a] Key laboratory of Marine Geology and Environment, Chinese Academy of Sciences, Qingdao 266071, PR China
[b] Institute of Oceanology, Chinese Academy of Sciences, Qingdao 266071, PR China
[c] School of Earth and Ocean Sciences, University of Victoria, Victoria V8P 5C2, Canada
Published online: 13 Jun 2014.

To cite this article: Jian-ke Fan, Shi-guo Wu & George Spence (2015) Tomographic evidence for a slab tear induced by fossil ridge subduction at Manila Trench, South China Sea, International Geology Review, 57:5-8, 998-1013, DOI: 10.1080/00206814.2014.929054

To link to this article: http://dx.doi.org/10.1080/00206814.2014.929054

International Geology Review, 2015
Vol. 57, Nos. 5–8, 998–1013, http://dx.doi.org/10.1080/00206814.2014.929054

Taylor & Francis
Taylor & Francis Group

Tomographic evidence for a slab tear induced by fossil ridge subduction at Manila Trench, South China Sea

Jian-ke Fan[a,b]*, Shi-guo Wu[a,b] and George Spence[c]

[a]*Key laboratory of Marine Geology and Environment, Chinese Academy of Sciences, Qingdao 266071, PR China;* [b]*Institute of Oceanology, Chinese Academy of Sciences, Qingdao 266071, PR China;* [c]*School of Earth and Ocean Sciences, University of Victoria, Victoria V8P 5C2, Canada*

(*Received 29 October 2013; accepted 26 May 2014*)

A tomographic travel-time inversion has been applied to trace the subducted slab of the South China Sea (SCS) beneath the Manila Trench. The dataset, taken from the International Seismological Centre (1960–2008), is composed of 13,087 P-wave arrival times from 1401 regional earthquakes and 8834 from 1350 teleseismic events. The results image the different morphology of the subducted SCS slab as a high-velocity zone. The subducting angle of the slab varies along the trench: at 16° N and 16.5° N, the slab dips at a low angle (24° ~ 32°) for 20–250 km depth and at a moderate angle (50°) for ~250–400 km depth. At 17° N, the slab dips at a low angle (32°) to near 400 km depth, and at 17.5° N and 18° N the slabs are near vertical from 70 ~ 700 km depth, while at 20° N the high-velocity anomalies exhibit features from horizontal abruptly to near vertical, extending to 500 km depth. The dramatic steepening of the slab between 17° N and 17.5° N may indicate a slab tear, which is coincident with the axis of a fossil ridge within the SCS slab at around 17° N. In addition, low-velocity zones in the three profiles above 300 km depth may represent the formation of the slab window, induced by ridge subduction and slab tear, initiating upward mantle flow and resulting in the partial melting of the edge of the slab. The slab tear could explain the volcanic gap and geochemical difference between the extinct Miocene and Quaternary volcanoes in the Luzon Arc, the much higher heat flow around the fossil ridge, and the distribution of most of the adakites and the related porphyry Cu-Au deposits in the Luzon area. Based on the geometry and morphology of the subducted slab and certain assumptions, we calculate the initial time of ridge subduction, which implies that ridge subduction and slab tear possibly started at ~8 Ma.

Keywords: tomography; ridge subduction; slab tear; Manila Trench; South China Sea

Introduction

The Philippine Archipelago probably resulted from processes of accretion, collision, subduction, arc volcanism, and ocean basin closure. It is located between two opposing subduction systems (Figure 1): to the west are the early Miocene Manila Trench, middle Miocene Negros Trench, and Cotabato Trench (e.g. Hayes and Lewis 1984; Mitchell *et al.* 1986; Rangin *et al.* 1999a; Yumul *et al.* 2008) and to the east are the Philippine Trench and East Luzon Trough, which are connected through an E–W-trending transform fault.

The Luzon Arc was generated by subduction of the SCS slab along the Manila Trench (Taylor and Hayes 1983). The Eurasian Plate collides directly with the arc at the northern and southern tips of the Manila Trench (e.g. Stephan *et al.* 1986; Suppe 1988; Teng 1990). The volcanoes in the Luzon Arc are divided into two volcanic chains by Yang *et al.* (1996): the Western Volcanic Chain (WVC), which continues along the western coast of the Luzon Island from Taiwan to Mindoro, and the Eastern Volcanic Chain (EVC), extending offshore in southeastern Taiwan to north of about 17.8° N (Figure 2). The two volcanic chains are separated by about 50 km at around 17.8° N and converge into a single volcanic chain northward. They are also diverse in age and chemical composition, and specifically the EVC volcanics are younger and more mantle-enriched. Yang *et al.* (1996) interpreted these variations as the effect of buoyancy of the subducted mid-oceanic ridge (MOR) within the SCS slab and a slab tear along the Continental–Oceanic Boundary (COB) of the SCS near 22° N (Figure 1). However, a refinement of Yang's model was presented by Bautista *et al.* (2001), who mainly used hypocentral and focal mechanism data to suggest that the tear occurs along the axis of the MOR of the SCS rather than the COB in Yang's model, and that the collision and subsequent partial subduction of a buoyant plateau at the margin near 20° N explains the abrupt change of the dip angle, the gap in the strain energy release, and the geochemical differences between the two volcanic chains in the Luzon Arc.

The abundance of earthquakes in this region resulting from the subduction at the trenches has allowed various seismic tomographic studies to be carried out (e.g. Fukao *et al.* 1992, 2001; Widiyantoro and Van der Hilst 1997).

*Corresponding author. Email: fanjianke_8888@163.com

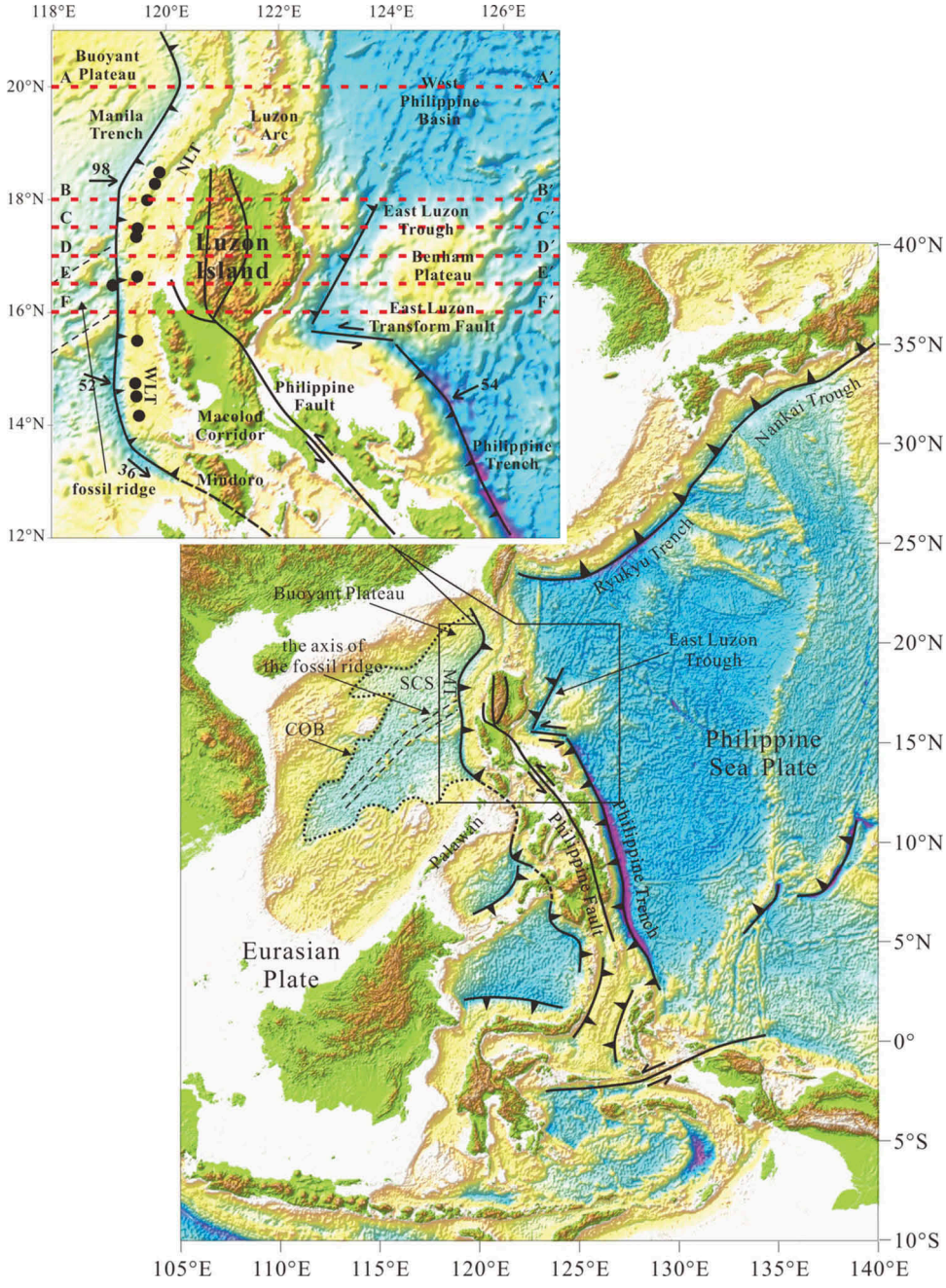

Figure 1. Tectonics in and around the Philippine region. The bathymetric data are from Smith and Sandwell (1997). The South China Sea (SCS) slab is a deep-water area enclosed by the dotted line and the Manila Trench. Black dots are the locations of the probe heat flow provided by Shi *et al.* (2003). Saw-toothed lines are subduction zones, dashed lines are collision zones, solid lines are faults, the double-dashed line is the inferred location of the fossil ridge of SCS, and red dashed lines are the location of profiles through the P-wave tomography model shown in Figure 10. The rectangle, indicating the inset location, represents the main study area imaged in the tomographic inversion and shown in Figures 3(A–B), 6, 8, and 9. NLT, North Luzon Trough; WLT, West Luzon Trough; COB, Continent–Ocean Boundary; SCS, South China Sea. The arrows and numbers denote the convergence rate (mm/year) along the subduction zone, which are from Rangin *et al.* (1999a).

However, these authors mostly concentrated on the Izu–Bonin–Mariana subduction zones, the eastern boundary of the Philippine Sea Plate. There are only a few papers involving the Manila subduction zone, the western boundary of the Philippine Sea Plate. By imaging the low-attenuation features, the subducted slabs related to the Manila and Philippine Trenches are estimated to extend to depths of 230 and 290 km, respectively

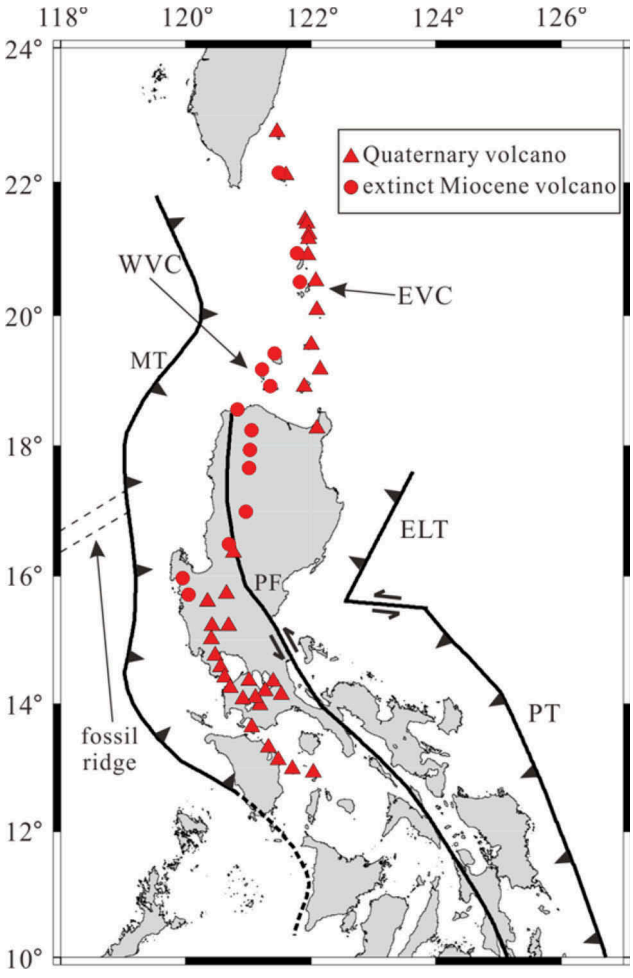

Figure 2. Volcano distribution in the Luzon Arc, on Luzon Island, and in the offshore to the north (modified from Yang *et al.* 1996). Saw-toothed lines are subduction zones, dashed lines are collision zones, solid lines are faults, and the double-dashed line is the inferred location of the fossil ridge of SCS. MT, Manila Trench; PT, Philippine Trench; PF, Philippine Fault; ELT, East Luzon Trough; WVC, west volcanic chain; EVC, east volcanic chain.

(Besana *et al.* 1997). Rangin *et al.* (1999b) and Lallemand *et al.* (2001) used the tomographic results of Bijwaard *et al.* (1998) to suggest that a vertical SCS slab, beginning at a depth of 100 km, could be overturned in the transition zone at 20° N. Beneath a profile normal to the Manila Trench at 18° N, Lallemand *et al.* (2001) also inferred that the SCS slab is disconnected from the surface at about 70 km depth, and at greater depths it dips shallowly eastward until about 300 km depth. They interpreted this as the subduction of the proto SCS slab, which was probably twice its present size.

Previous studies on the two opposing subduction systems examined the subducted SCS slab using geomorphological, geochronological, geochemical, and geophysical data, plus limited tomographic evidence. The most recent model focusing on the structure of the Luzon arc Bautista *et al.* (2001) was mainly based on detailed profiles of earthquake distribution, but did not incorporate tomographic interpretations. To carry out the seismic tomography in this paper, we utilized a P-wave arrival time data set collected over the last five decades, which is larger than that used in previous works. We focused on the morphology of the subducted SCS slab and integrated the results with other geological, geophysical, and geochemical data to verify the slab tear along the fossil ridge of SCS. Our results provide new insight into the interaction between the SCS slab and Philippine Sea Plate, and help in understanding the tectonics and evolution of the Eurasian Plate and Philippine Sea Plate.

Data and methods

The data used in this study are P-wave arrival times, which are an edited version (EHB bulletin) from the International Seismological Centre (ISC) (Engdahl *et al.* 1998) for earthquakes occurring between 1960 and 2008. The average mislocation vector of the data set is 9.4 ± 5.7 km, which was achieved by using the ak135 1D travel-time model, iterative relocation with dynamic phase identification, first-arriving P, S, and PKP phases, the teleseismic depth phases pP, pwP, and sP, ellipticity corrections for the ak135 model, and empirical teleseismic station patch corrections (for 5° × 5° patches).

The data set was composed of two parts: the regional earthquakes and the teleseismic events. The criteria for selecting the earthquakes used in this study were as follows: (1) each earthquake was recorded by over five stations located in the study area; (2) the absolute value of the travel-time residuals was lower than 5 s; (3) the arrival time reading precision was lower than 0.1. Also, the distance from the centre of the study area to a teleseismic event was restricted to the range 30°–100°, in order to avoid the influence of the complex structures in the lowermost mantle and in the upper mantle outside the study region (Zhao *et al.* 1994, 2013). After selection, there was a total 13,087 arrival times from 1401 regional earthquakes and 8834 arrival times from 1350 teleseismic events. Figure 3 shows the distribution of the earthquakes and the 51 seismic stations used in this study.

For the teleseismic events, relative travel-time residuals were used to avoid the effects of hypocentral mislocation and origin times, and the complex structures outside the study region (Zhao *et al.* 1994). First, the IASP91 Earth Model (Kennett and Engdahl 1991) was utilized to calculate the theoretical travel times between the hypocentre and the recording stations, and the raw travel-time residuals were subsequently computed by eliminating the theoretical travel times from the observed. After that, we obtained the relative travel-time residuals for each event from the raw ones by removing the mean

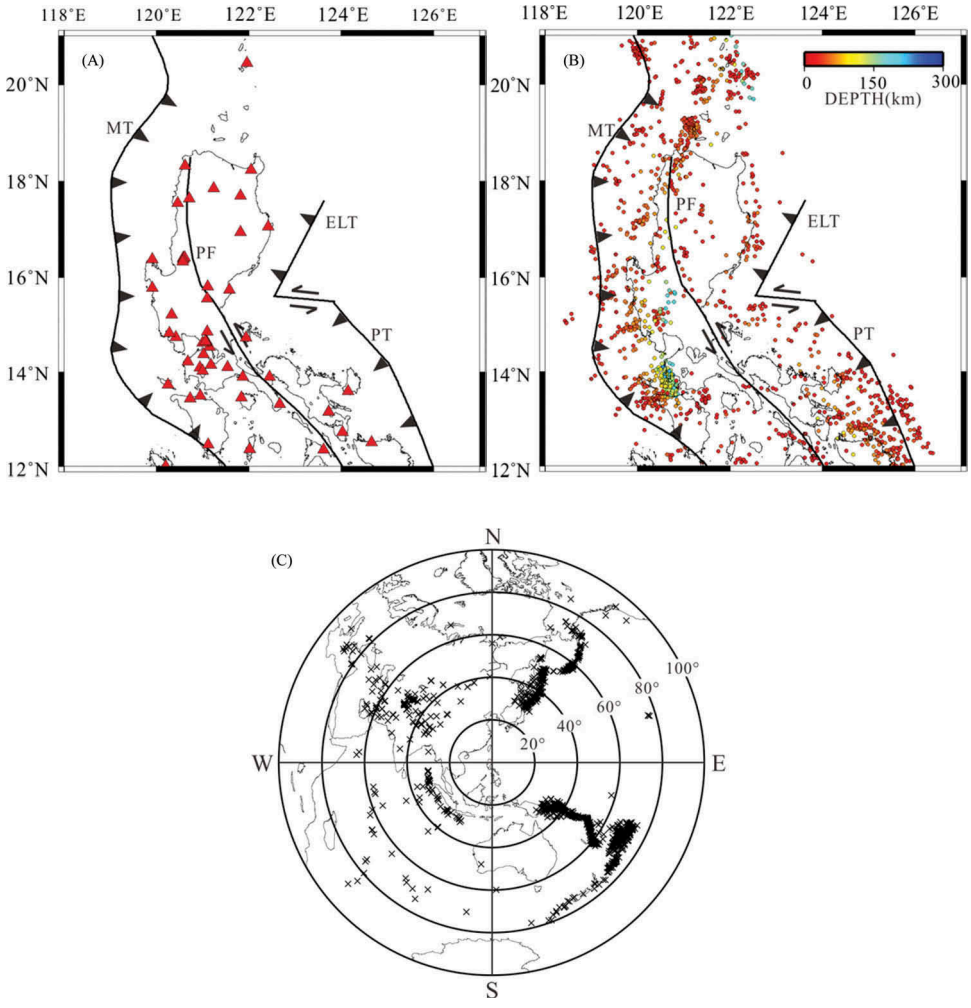

Figure 3. (A) Distribution of the stations (red triangles) used in this study. (B) Regional earthquakes (dots) used in this study. Colours denote earthquake focal depth. (C) Teleseismic events (black crosses) used in this study. Saw-toothed lines are subduction zones, dashed lines are collision zones, and solid lines are faults. MT, Manila Trench; PT, Philippine Trench; PF, Philippine Fault; ELT, East Luzon Trough.

residual, which was calculated by averaging over all recording stations.

The seismic tomographic method of Zhao *et al.* (1992, 1994) for local and teleseismic joint inversion was used to obtain the P-wave velocity perturbations beneath Luzon Island. Travel times and ray paths were computed using an efficient 3D ray tracing technique, within which the pseudo-bending technique (Um and Thurber 1987) and Snell's law were introduced. Velocity discontinuities, such as Conrad, Moho, and 410 km discontinuities, were also introduced into the initial model, which can effectively reduce travel-time residuals. For local events, their raw travel-time residuals were used in the tomographic inversion while the relative travel-time residuals were used for the teleseismic events. The tomographic inverse problem was solved by iteratively applying the damped least-squares routine (LSQR; Paige and Saunders 1982) to solve the large and sparse system of observation equations.

Model parameterization and inversion

A one-dimensional (1D) initial model (Figure 4) was derived from the models CRUST2.0 (Bassin *et al.* 2000), IASP91 (Kennett and Engdahl 1991), and WPSP01P (Wright and Kuo 2007; Wright 2009). Inversion for both oceanic and continental crustal structure resulted in dramatic undulations in Moho depth, and therefore the crustal thickness and velocities from the CRUST2.0 model were introduced into the starting velocity model, which significantly reduced the travel-time residuals. The Conrad depth ranged from 4 to 22 km, whereas the Moho depth ranged from 8 to 33 km. The WPSP01P model depicts the velocity of the upper mantle and transition zone below the Luzon region, defined by the earthquakes south of Taiwan as recorded by seismic stations within and around Taiwan. Wave speeds above 130 km in the WPSP01P model were lower than those in the IASP91 model, and they increased linearly rather than remaining mainly constant. Our initial

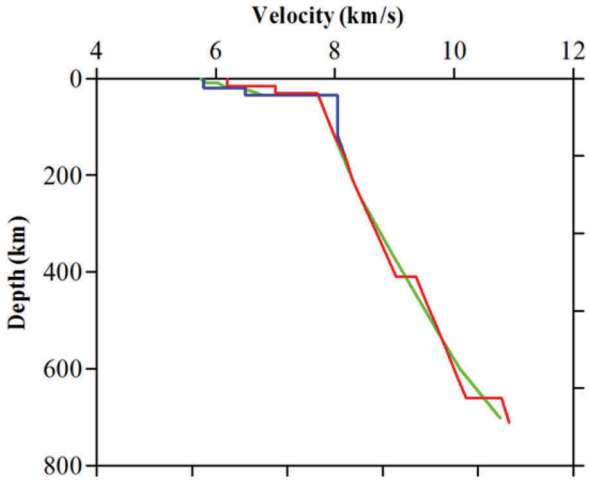

Figure 4. Initial P-wave velocity model used in the study (red line), IASP91 (blue line) (Kennett and Engdahl 1991), and WPSP01P model (green line) (Wright and Kuo 2007; Wright 2009).

model used the upper mantle wave speeds of WPSP01P to 210 km depth, and the IASP91 model for velocities at depths over 210 km.

A three-dimensional (3D) grid was set up in the modelling space to express 3D velocity variations. Grid intervals in the longitudinal, latitudinal, and depth directions affect the resolution of the tomographic image; 0.5° was found to be the optimal grid interval in the longitudinal and latitudinal directions for our data set after many tests. In the depth direction, the grid node meshes were at depths of 5, 20, 50, 100, 150, 200, 250, 300, 400, 500, 600, and 700 km.

The final tomographic results are heavily affected by the values of the damping and smoothing parameters, which can be obtained by conducting many tomographic inversions with different values of the damping and smoothing parameters to compare the relationship between the variance of velocity perturbations and root mean square (RMS) travel-time residuals. The optimal values of the damping and smoothing parameters were selected as 5.0 and 500.0, respectively (Figure 5), in order to balance the reduction of travel-time residuals and the smoothness of the 3D velocity model (Eberhart-Phillips 1986). The final velocity model and the travel-time residuals did not change significantly after the third iteration. At this point, the RMS of travel-time residuals was reduced from 1.46 s in the initial model to 0.72 s in the final model.

Resolution and results

Checkerboard resolution test

To confirm the main features of the tomographic results, we conducted a checkerboard resolution test (CRT) with grid spacing of 0.5°. In the CRT, we first added perturbations of ±3% to the 3D grid nodes to construct a perturbed model that served as the input model, then calculated the synthetic arrival times with the same source-receiver geometry. Finally the synthetic arrival times were inverted for the output model starting at the initial model, without any perturbations. By comparing the input with the output model, we can determine the resolution in the model space. Figure 6 shows the results of a CRT with a grid spacing of 0.5° × 0.5° at different depths. At 5 km depth, the resolution is good only on Luzon Island due to the absence of earthquakes and stations in the oceanic region. From 20 to 300 km depth, most of the study area has good resolution, especially beneath Luzon Island and its offshore area just to the west. In most of the oceanic areas east of Luzon Island, the resolution is poor due to the absence of sufficient ray paths. Deeper than 400 km, the resolution is good for the eastern part of the study area, which corresponds to the region with good ray coverage, in contrast to the region from 118° to 122° E, where ray coverage is poor (Figure 7(B)). Lévêque *et al.* (1993) showed that in CRT, larger-size structures are poorly

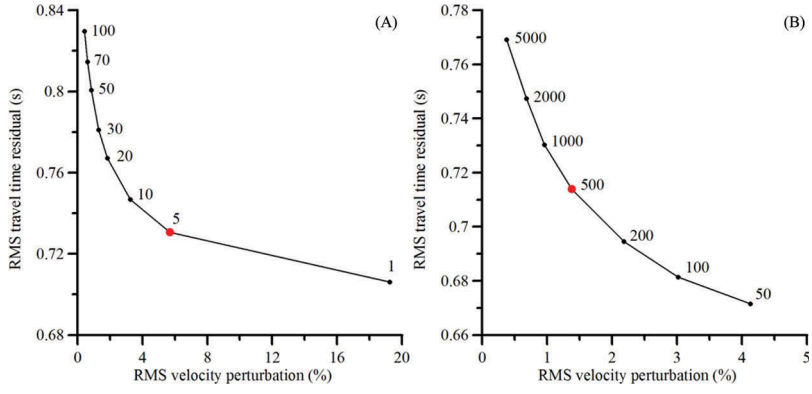

Figure 5. Trade-off curves for the variance of root mean square (RMS) velocity perturbations and travel-time residuals, with different values of the damping parameter (A) (the numbers beside the circles) and the smoothing parameter (B) (the numbers beside the circles). The red circles denote the optimal damping parameter in (A) and smoothing parameter in (B).

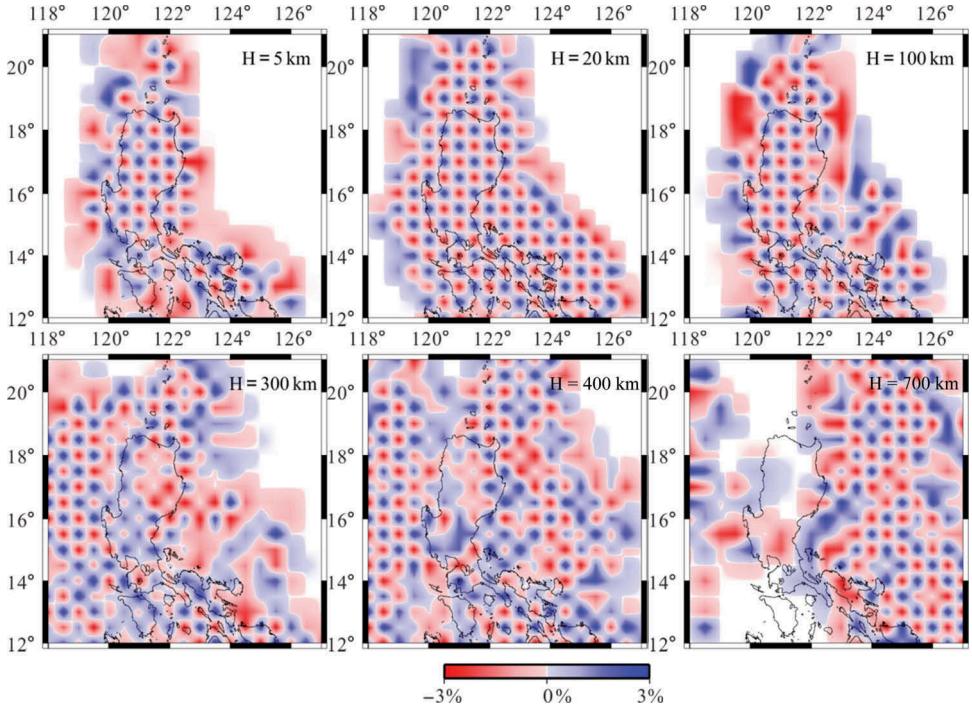

Figure 6. Checkerboard resolution tests for six depth layers with a grid of 0.5° in the longitudinal and latitudinal directions. The depth of each layer is shown at the top right corner of each map, and the velocity perturbation scale is shown at the bottom.

recovered even though there is good resolution at small scales. Therefore we also conducted a CRT with a grid spacing of 0.7° × 0.7°, and the result is consistent with that using a grid spacing of 0.5° × 0.5°, showing that the checkerboard pattern is recovered very well for most parts of the modelling space (Figure 8).

Results

Velocity perturbations with the grid of 0.5° × 0.5° obtained by our tomographic inversion are presented in Figures 9 and 10, in which the location of six profiles is shown in Figure 1.

The tomographic results are similar at both 5 and 20 km depth (Figure 9(A–B)). The most striking feature is the existence of a large area of low-V anomalies, most of which lie precisely beneath the volcanoes in the Luzon Arc from south of Taiwan to Mindoro. Distinct from the above results, high-V anomalies are prominent below 50 km depth (Figure 9(C–F)), and are believed to be related to the subducted plate along the trenches. At 50 km depth (Figure 9(C)), most of the high-velocity anomalies are situated in the vicinity of the trenches (i.e. the Manila Trench, East Luzon Trough, and Philippine Trench). The high-velocity anomalies beneath the west coast of Luzon Island belong to the subducted SCS slab along the Manila Trench, with those beneath the east coast of Luzon Island belonging to the subducted Philippine Sea Plate along the East Luzon Trough and Philippine Trench. From 100 to 200 km depth (Figure 9(D–E)), the high-velocity anomalies belonging to the subducted SCS slab are divided into several parts. North of the fossil ridge of the SCS, the high-V anomalies are far from the Manila Trench, while in contrast, the high-V anomalies south of the fossil ridge are still adjacent to the Manila Trench.

Profile FF′ (Figure 10(F)) at 16° N shows a high-velocity zone dipping east initially at a low angle of about 24° and then at a higher angle of about 50° to about 400 km depth, coincident with the tendency of most of the seismicity beneath the forearc region of Manila Subduction Zone. Another high-velocity zone, located from 121.5° to 123.5° E above 100 km depth, is interpreted as the subducting Philippine Sea Plate along the East Luzon Trough. The shallow subduction depth may indicate that the present East Luzon Trough is a relic of the proto-East Luzon Trough (Hamburger *et al.* 1983).

Similar to profile FF′, profile EE′ (Figure 10(E)) at 16.5° N shows that the SCS slab subducts initially along the Manila Trench to 250 km depth at a low angle of about 30°, and then the dip changes to a higher angle (~50°) to about 450 km depth, which is consistent with the trend of the earthquake foci. However, there is only a hint of a high-velocity anomaly representing the subducted Philippine Sea Plate along the East Luzon Trough, which suggests that the East Luzon Trough is active only at the southern tip.

Different from profiles EE′ and FF′, profile DD′ (Figure 10(D)) at 17° N shows that the high-velocity

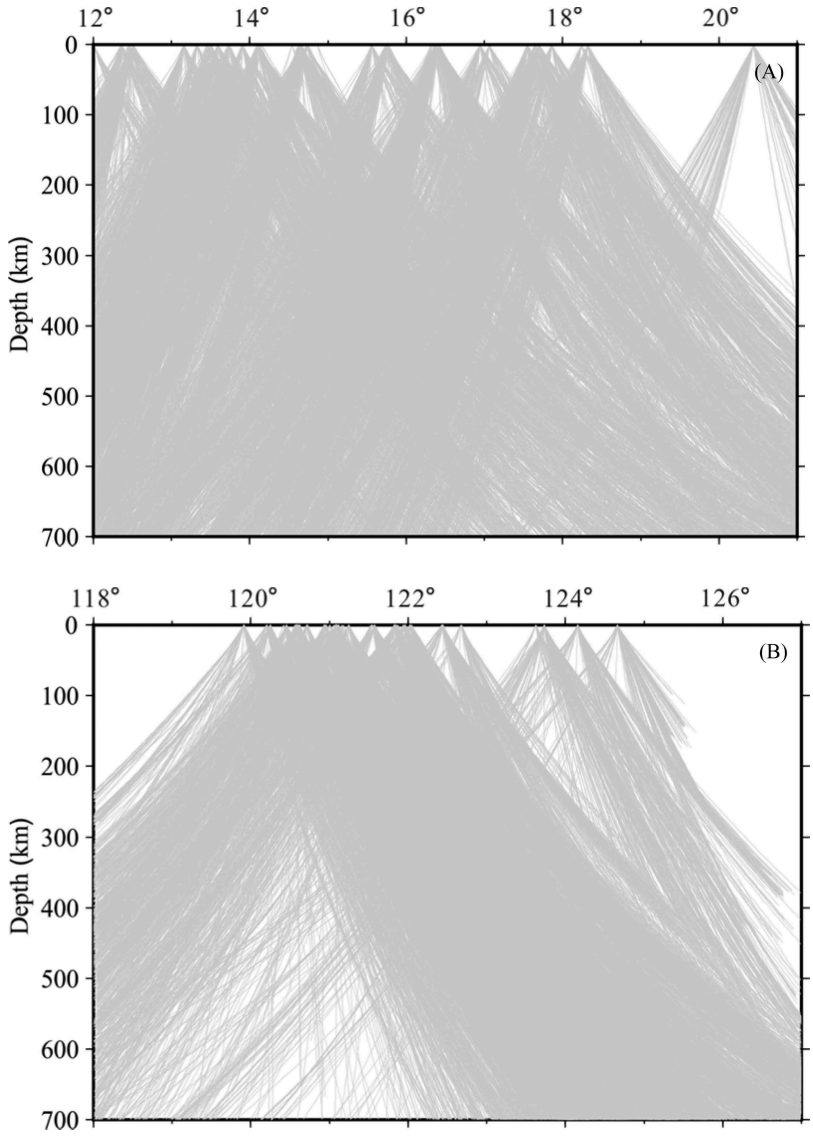

Figure 7. East–west (A) and north–south (B) vertical cross-sections of P-wave ray paths (grey lines) from 1401 regional earthquakes and 1350 teleseismic events used in this study.

zone representing the subducted SCS slab with a low angle of ~32° is discontinuous, which may be attributed to the low-velocity zone beneath the high-velocity zone (the region outlined in red in Figure 10(D)), as discussed below.

In profiles CC′ and BB′ (Figure 10(B–C)), the high-velocity anomalies extend to about 700 km depth at a near-vertical angle, suggesting that the SCS slab subducted vertically downwards to the transition zone. The subducted SCS slab is divided into two high-velocity segments, and between these are wide, low-velocity anomalies. High-velocity anomalies associated with the subducted PSP along the East Luzon Trough vanish in profiles BB′, CC′, and DD′, consistent with the northward termination of seismicity at around 17°–18° N.

In profile AA′ (Figure 10(A)), the high-V anomalies exhibit a horizontal feature above 100 km depth, and then abruptly vary to near vertical, extending to near 500 km depth. Our tomographic results in this profile are consistent with other previous tomographic results at the same latitude (Lallemand *et al.* 2001; Koulakov *et al.* 2014).

To further confirm our inversion results, we conducted synthetic tests. We first modified the inversion results to produce a much simplified input model, mainly including a dipping, slab-like high-velocity zone and an adjacent, approximately circular, low-velocity zone (Figure 10(A′–F′)). We then calculated the synthetic arrival times using this input model with the same source-receiver geometry as the final model. Subsequently, we inverted the synthetic arrival times for an output model starting at the same 1D initial model as in

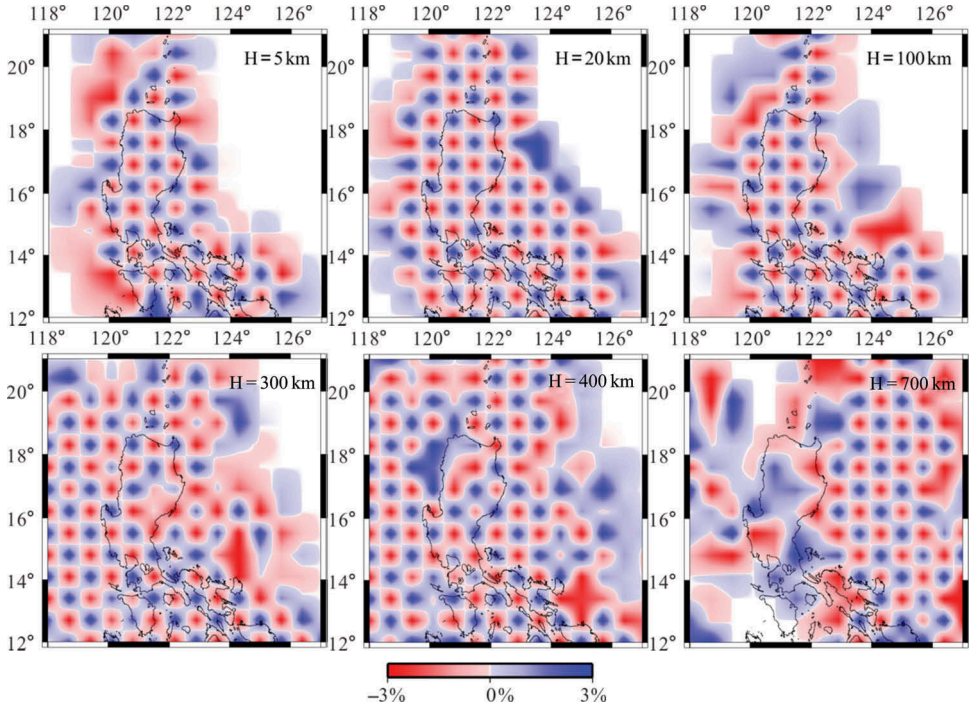

Figure 8. Checkerboard resolution tests for six depth layers with a grid of 0.7° in the longitudinal and latitudinal directions. The depth of each layer is shown at the top right corner of each map, and the velocity perturbation scale is shown at the bottom.

our real inversion. The results of this synthetic test (Figure 10 (A′–F′)) show that the geometry and amplitude of both the high- and low-velocity features are reproduced remarkably well. As might be expected, there is some smearing of the boundaries of the features, and the amplitudes of the features are reduced from the true values of 6% velocity perturbation to 3–4%.

Discussion

Seismic velocity structure indicating slab tear

Ridge subduction is very common in the Pacific margin region. Usually, the occurrence of ridge subduction is associated with interpretations of slab tear or the formation of a slab window (e.g. Thorkelson and Taylor 1989; Madson *et al.* 2006; Zandt and Humphreys 2008; Russo *et al.* 2010). Based on body-wave travel-time tomography, the P-wave structure of the subducted Chile Ridge between the Nazca and Antarctic plates shows a distinct low-velocity zone relative to surrounding asthenospheric mantle. It is inferred as being filled by unusually warm asthenosphere, consistent with subduction of the Chile Ridge (Russo *et al.* 2010). In addition, aseismic ridge subduction has been linked with other considerable changes in the geometry and kinematics of both the subducting and overriding plates, such as reduction of the slab dip or a gap in arc volcanism (Rosenbaum and Mo 2011; Martinod *et al.* 2013).

Our tomographic results depict the 3D geometry and morphology of the subducted SCS slab along the Manila Trench. Our results beneath three east–west profiles from 16° to 17° N image the subducting slab as a distinct high-velocity zone dipping eastwards from the Manila trench to near 400 km depth. However, between 17° and 17.5° N, the dip angle changes abruptly from low values of 24° ~ 32° to near-vertical. This dramatic change in dip angle can be interpreted as indicating a tear of the subducted SCS slab at ~17° N (Figure 11). These images of velocity structure provide independent support for a similar slab structure interpreted by Bautista *et al.* (2001), based on the detailed distribution of regional earthquake hypocentres. The occurrence of a possible slab tear is consistent with the subduction at 17° N of a fossil ridge at the Manila trench, as suggested by Bautista *et al.* (2001). In addition, the dip angle of the subducted slab generally decreases northward from 16° to 17° N (Figure 10(D–F)). Some geodynamic models (e.g. Pilger 1981; Martinod *et al.* 2005, 2013; Espurt *et al.* 2008) have discussed the effect of the subduction of high bathymetric relief, including aseismic ridges, which can lead to shallowing of the subducting dip angle, and even to flattening of the slab at characteristic depths of ~100 km if the convergence velocity is very high (Figure 10(A), Gutscher *et al.* 2000; Van Hunen *et al.* 2002; Martinod *et al.* 2013). The low angle subduction of the SCS slab around the fossil ridge could be attributed to the buoyancy of the ridge.

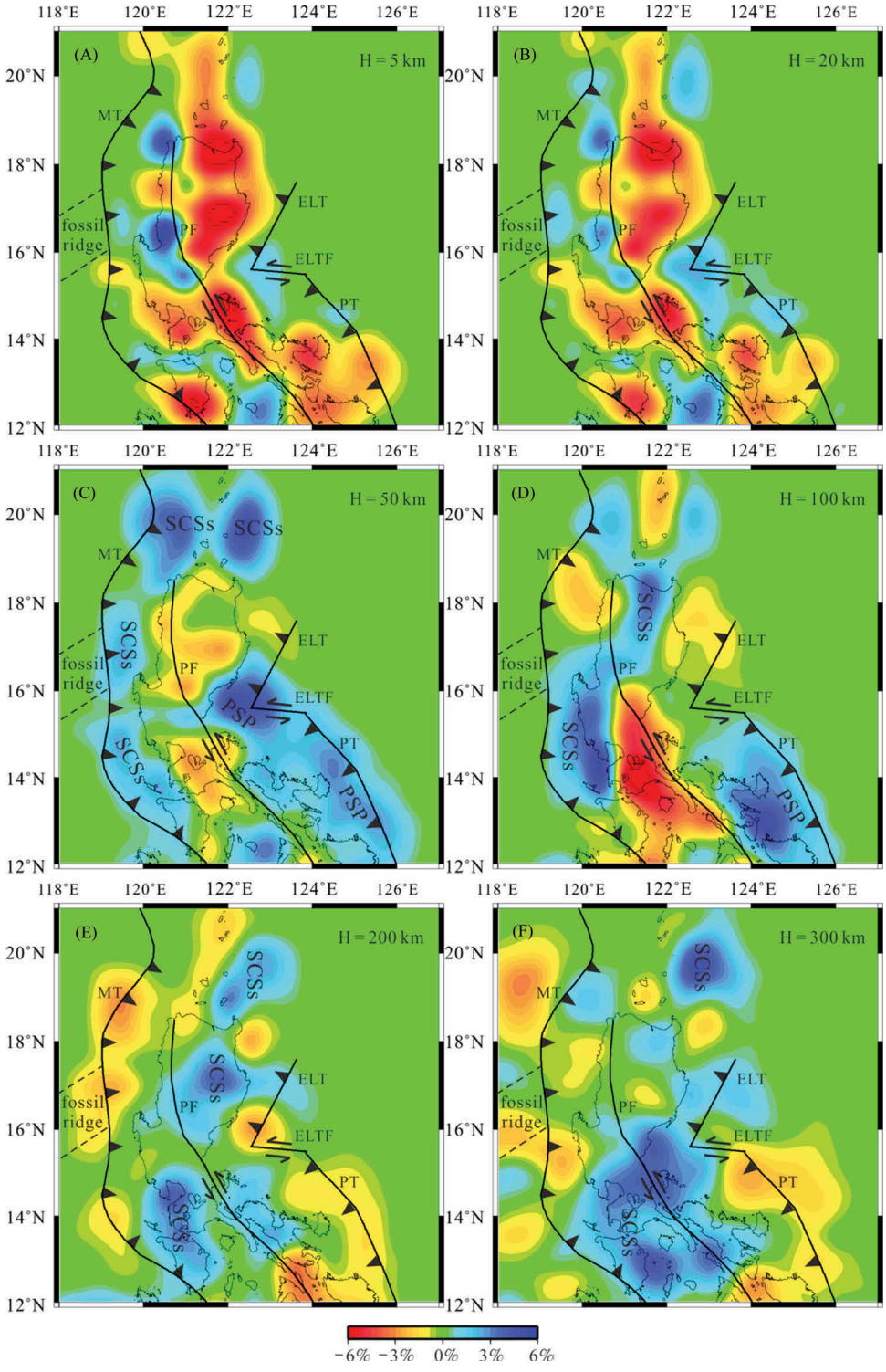

Figure 9. P-wave velocity perturbations relative to the initial model of Figure 4 at different depths, each of which is shown at the top right corner of each map. Red and blue denote slow and fast velocity perturbations, respectively. The velocity perturbation scale is shown at the bottom. Subduction zones, collision zones, and faults are expressed by saw-toothed, dashed, and solid lines, respectively; the double-dashed line is the inferred location of the fossil ridge of SCS. MT, Manila Trench; PT, Philippine Trench; PF, Philippine Fault; ELT, East Luzon Trough; ELTF, East Luzon Transform Fault; SCSs, South China Sea slab; PSP, Philippine Sea Plate.

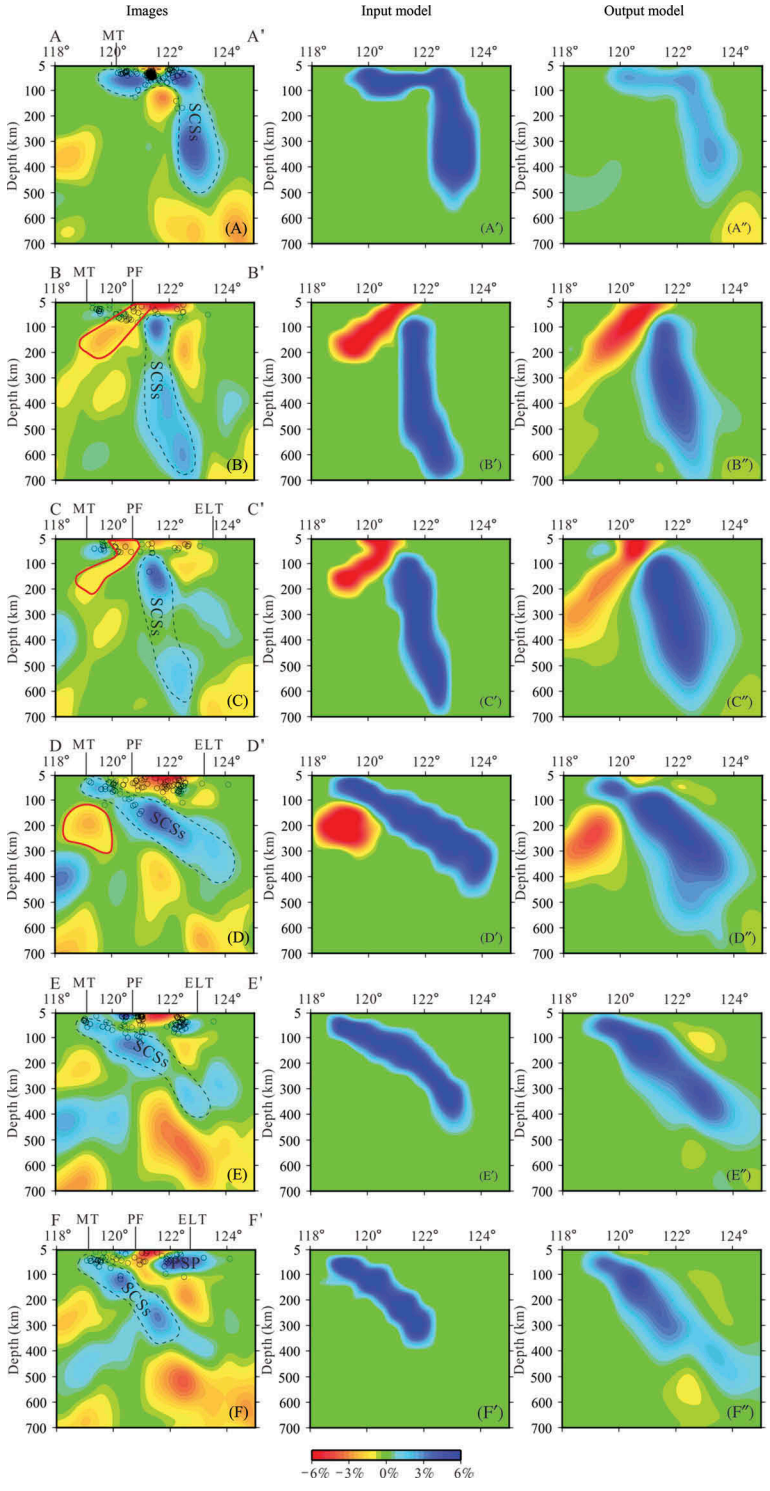

Figure 10. P-wave velocity perturbations relative to the initial model of Figure 4 along the profiles shown in Figure 1. The left-hand panels (A–F) show the tomographic images obtained in six profiles. For synthetic models shown in the middle panels (A′–F′), travel times were calculated using the same source-receiver geometry as in the real data. These travel times were inverted to give the output models shown in the right-hand panels (A′–F′). The velocity perturbation scale is shown at the bottom. White dots represent the projection of earthquakes occurring within 15 km of each profile. The black dashed lines denote the speculated morphology of the subducted SCS slab, and the red solid lines outline the region of a speculated slab window containing hot mantle from the slab tear. MT, Manila Trench; ELT, East Luzon Trough; PF, Philippine Fault; PT, Philippine Trench; SCSs, South China Sea slab; and PSP, Philippine Sea Plate. The locations of profiles A–F are at 20°, 18°, 17.5°, 17°, 16.5°, and 16°, respectively. The vertical exaggeration is 1:1.

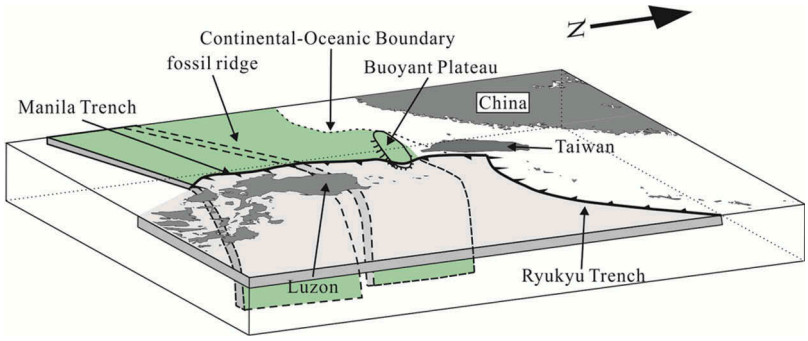

Figure 11. Schematic map of the morphology of the subducted South China Sea slab along the Manila Trench.

In profiles BB′ and CC′ (Figure10(B–C)), there is no obvious high-velocity anomaly representing the subducted SCS slab above 100 km depth. We suggest that this implies flat subduction of the fossil ridge of SCS slab above 100 km from 119° to 121° N (Gutscher *et al.* 2000; Van Hunen *et al.* 2002; Martinod *et al.* 2013) due to the buoyancy of the ridge at 17° N and the buoyant plateau at around 20° N (Figure 10(A)). No high velocities are seen, since the ridge would allow hot upper mantle material to infill this shallow region, as indicated by the low-velocity zone at 17.5° and 18° N (the regions outlined in red in Figure 10(B–C)). Similarly, at 17° N (Figure 10(D)), our tomographic results reveal that the high-velocity anomalies are discontinuous at around 120° E, which may be due to the influence of the ridge. The fossil ridge itself may be very fragile, which is suggested by the low coupling ratio derived from the trench parallel gravity anomaly at around 17° N (Hsu *et al.* 2012), so that the fossil ridge in general may be a stress weak zone that can easily tear.

Slab tear, slab windows, and geochemistry of volcanics

Another dramatic response to ridge subduction is the formation of volcanic gaps (Rosenbaum and Mo 2011), such as those recognized in Peru and central Chile. Besides the volcanic gap recognized by Yang *et al.* (1996), we also note that there is a volcano gap among the Quaternary volcanoes located between 15.5° and 17.5° N (Figure 2), precisely the location of the subducted fossil ridge of SCS. Therefore, the volcanoes since the Quaternary can be divided into a northern and a southern segment. The distance between the northern segment (i.e. Eastern Volcano Chain) and the trench is greater than that between the southern segment and the trench. This may be attributed to the subduction of the fossil ridge and the buoyant plateau at around 20° N, in agreement with our tomographic results, which show that in general the dip of the subducted SCS slab decreases northward.

The tearing of the lithospheric slab in response to aseismic ridge subduction can develop slab windows, producing a series of magmatic centres along tear faults where magmatism is generated by asthenospheric upwelling. The result is considerable heating in the forearc region and near-trench magmatism. The heat flow data provided by Shi *et al.* (2003) (Figure 1) reveal that the heat flow is much higher (>100 mW m^{-2}) along the axis of the MOR of the SCS east of the Manila Trench than that at the adjacent two troughs (<50 mW m^{-2} at both the West Luzon Trough and North Luzon Trough). This high-heat flow region, plus the low-velocity zones from the seismic tomography in the same area (Figure 10, red-outlined regions), are consistent with the existence of the slab window.

Examples from the Mediterranean region (e.g. Rosenbaum *et al.* 2008; Gasparon *et al.* 2009) show that the magmas produced in slab windows will have transitional geochemical signatures between arc type and ocean island basalt type (Maury *et al.* 2000; De Astis *et al.* 2006). The magmas of the extinct Miocene volcanoes of the Luzon arc have low K, large ion lithophile element, light rare earth element, and Th/U ratios (Defant *et al.* 1989; Defant and Drummond 1990), while the Quaternary volcanoes have higher ratios, especially in the EVC. We suggest that the slab tear of the SCS slab along the extinct MOR and the subduction of the buoyant mass at around 20° N affect the geochemistry of the volcanoes since Quaternary.

Adakite and adakitic rocks, as defined by Defant and Drummond (1990), are regarded as the partial melting of young subducted slab (<25 Ma). However, thermal models suggest that melting a of subducting slab in modern subduction zones is only likely to occur when it is very young (<5 Ma; Peacock *et al.* 1994) (i.e. the active mid-ocean ridge; Pe-Piper and Piper 1994; Thorkelson 1996; Thorkelson and Benoit *et al.* 2002; Breitsprecher 2005). Adakites are very common in the Luzon Arc, and most are believed to be related to plate subduction of the SCS, the Sulu Sea, the Celebes Sea, and the Philippine Sea (Figure 11). Nevertheless, the relatively old age of the subducting SCS slab makes it difficult to melt except at the edge of a torn subducting plate. Equivalent examples of older plates producing adakites are found in New

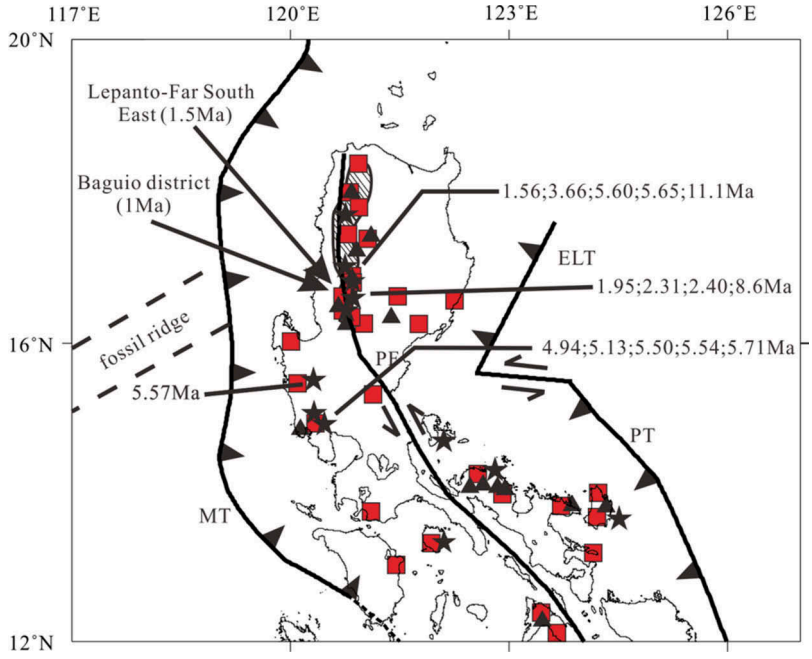

Figure 12. Schematic map of the distribution of copper and gold deposits and adakite rocks (modified from Sajona and Maury 1998; Cooke *et al.* 2005). The red rectangles denote the sites of copper deposit, black triangles denote gold deposits, and stars denote adakite rocks. The slashed shadow zone is the gold/copper district or province. Saw-toothed lines represent subduction zones, dashed lines are collision zones, and solid lines are faults. MT, Manila Trench; PT, Philippine Trench; PF, Philippine Fault; ELT, East Luzon Trough. Lepanto-Far South East and Baguio district are two sites of giant porphyry deposits whose formation ages are denoted by the numbers. Other numbers are the K–Ar ages of the adakite and adakitic rocks related to the subduction of the SCS slab along the Manila Trench.

Zealand's South Island (Reay and Parkinson 1997), Costa Rica (Johnston and Thorkelson 1997), and Kamchatka Peninsula and the Aleutian Islands (Yogodzinski *et al.* 2001). The adakites in Northern and Central Luzon, associated with the eastward subduction of the SCS slab (34–17 Ma), have previously been interpreted as originating from partial melting of the lower Luzon crust (Yumul *et al.* 2000; Bellon and Yumul 2001). In our interpretation of the seismic velocity results, slab tear along the fossil ridge produces low-velocity zones from the surface to 200 km depth (red-outlined regions in Figure 10(B–D)), which are associated with hot mantle flowing upwards and producing partial melting of the edge of the slab and lower crust. This interpretation is consistent with previous explanations for the existence of adakites landward of the fossil ridge.

Most porphyry Cu–Au deposits globally are considered to be related to adakites (Oyarzun *et al.* 2001; Reich *et al.* 2003) and hence to the subduction of ridges (Cooke *et al.* 2005). This has also been proposed for Cu–Au deposits in the Philippines (Sajona and Maury 1998). As moderately incompatible elements, Cu and Au are enriched much more in the oceanic crust than in the continental crust and the mantle. When the partial melting of young (<5 Ma) oceanic crust occurs during subduction, Cu and Au are then involved in mantle convection and concentrate in the ore formation, similar to the process and conditions that formed the adakites. In Northern Luzon, there are two giant porphyry Cu–Au deposits formed at ca. 1–1.5 Ma, which are located in the subduction axis of the extinct MOR of the SCS slab, where adakites have been enriched since the subduction of the MOR at around 2 Ma (Figure 12). Therefore, there is a relationship between the Cu–Au deposits and the adakites, both of which are generated by tearing of the SCS slab along the axis of the MOR during ridge subduction.

Timing for subduction of fossil ridge region

The Luzon block has undergone a counterclockwise rotation resulting from the northwestward movement of the Philippine Sea Plate, the collision of the Palawan microcontinental block with the Philippine Mobile Belt, and the collision of the Luzon arc with the Eurasian Plate margin (Rangin *et al.* 1999a). With current structure based on tomographic results, Lallemand *et al.* (2001) assumed oblique convergence between the north-northeast extinct MOR and the Philippine Sea plate and showed that the original size of the SCS plate was about twice its present size. Thus, subduction of the SCS slab accompanying the northwestern movement of the Philippine Sea Plate also supports retreat of the Manila Trench.

In the light of our tomographic results, we propose some refinements to the geodynamic models of Yang *et al.*

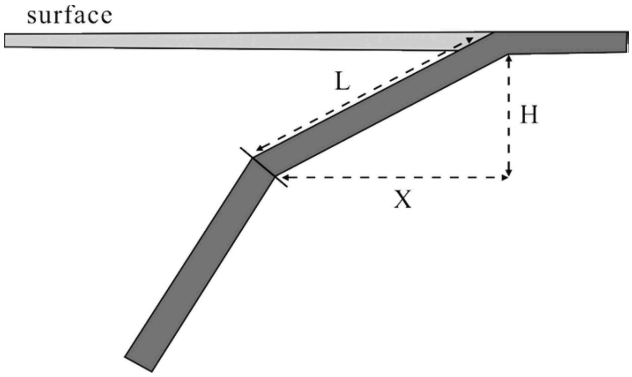

Figure 13. Diagram for calculating the length of a subducting slab. L is the distance from the trench to a certain depth of the subducting slab, H is the vertical distance from the surface to a certain depth, while X is the horizontal distance of the subducting slab.

(1996) and Bautista *et al.* (2001) to calculate the subduction time of the fossil ridge region, which is constrained by the subducted time of the low-angle (24° ~ 32°) pattern of the subducted plate (L_1 as illustrated in Figure 13). According to Martinod *et al.* (2013), because of buoyancy, the subduction of a ridge will affect a region to subduct at a lower angle around the ridge. The initial time of ridge subduction can be calculated according to the lower-angle subduction segment at different latitudes. According to the Pythagorean theorem, we can obtain the length of the subducted slab affected by the subduction of the fossil ridge followed by $L = \sqrt{X \times X + H \times H}$, which is about 300, 420, or 640 km at 16°, 16.5°, or 17° N, respectively. The convergence rate at the Manila Trench, provided by Rangin *et al.* (1999a), is assumed to increase linearly from ~52 mm/year at 15° N to ~98 mm/year at 18.2° N (Figure 1), so convergence rates at 16°, 16.5°, and 17° N are interpolated to give values of 66, 74, and 81 mm/year, respectively. If the convergence rate is constant during subduction, then the ridge subduction times at 16°, 16.5°, and 17° N are ~4.5, ~5.6, and ~7.9 Ma, respectively. At 17.5° N, the slab is subducted horizontally above 100 km depth, and the length and convergence rate are about 220 km and 88 mm/year, respectively. Then, the ridge subduction time at 17.5° N is ~2.5 Ma, coinciding with the time of subduction of the buoyant plateau proposed by Bautista *et al.* (2001). Yang *et al.* (1996) argued that at around 6 Ma the fossil ridge was approaching the Manila Trench, and at 4 ~ 5 Ma, the fossil ridge had already accreted to the Manila Trench and caused the cessation of slab subduction. Then, at around 2 Ma, subduction of the slab resumed. However, our ridge subduction times suggest that ridge subduction has been sustained since ~8 Ma, merely at different latitudes. Yang *et al.* (1996) did not consider the retreat of the Manila Trench, the northwestward movement of the Luzon Arc, and the size of the SCS slab before subduction. Consequently, we argue that the fossil ridge of SCS may have been subducted along the Manila Trench since 8 Ma. Due to the collision between the Palawan block and Luzon Island and the northwestward movement of the Philippine Sea Plate, the Manila Trench rotates counterclockwise accompanying Luzon Island. Supposing that the subducted ridge extended NE–SW as it is now, then ridge subduction began from the northeastern part and propagated to the southwest (Figure 14). Once the ridge

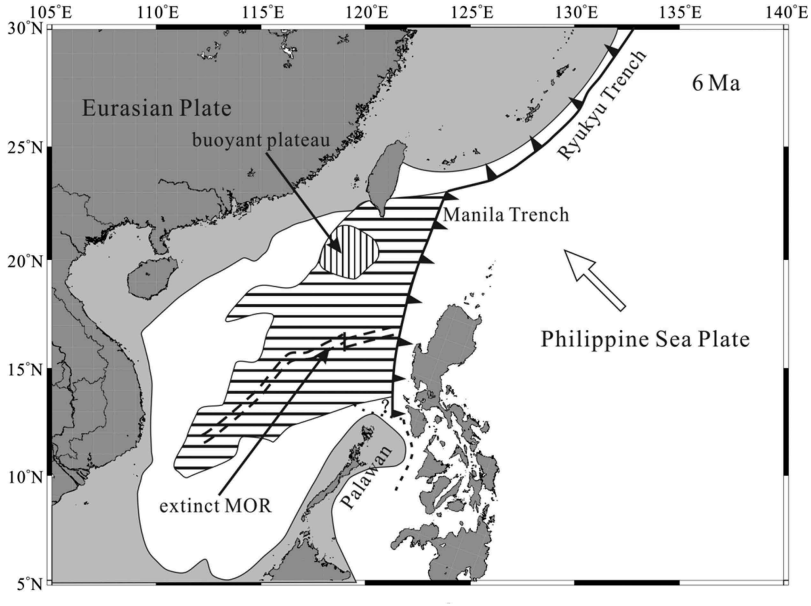

Figure 14. Schematic map of the evolution of the South China Sea slab and Philippine Sea Plate at ~6 Ma.

subducted, our tomographic model suggests that the SCS slab may have torn along the axis of the ridge and melted partially at the edge of torn slab, consistent with the existence of adakites. At ~3 Ma, the buoyant plateau collided with the Manila Trench and subducted, possibly leading to flat subduction of SCS slab and formation of the East Volcanic Chain (Figure 11).

Conclusions

The tomographic results obtained from inverting 1401 regional earthquakes and 1350 teleseismic events in and around the Luzon area depict the three-dimensional geometry and morphology of the subducted SCS slab along the Manila Trench. The dip angle at 17.5° N is significantly different from that at 17° N, indicating that the slab tore along the axis of the fossil ridge of the SCS. Ridge subduction results in low-angle subduction of the SCS slab near the ridge and the formation of a volcanic gap. The slab window, induced by slab tear, is indicated by low-velocity anomalies in three profiles through our tomographic model. A region of high heat flow in the forearc, adakites, and porphyry Cu–Au deposits in Northern Luzon is attributed to the tearing of the SCS slab along the fossil ridge, initiating the upward mantle flow and resulting in the partial melting of the edge of the slab and lower crust Based on the geometrical character of the subducted slab, we calculated the time of ridge subduction, which implies that the ridge subduction and slab tear possibly started at ~8 Ma. We propose a geodynamic model to explain the evolution of the slab tear, which suggests that the fossil ridge of the SCS slab subducted beginning at ~8 Ma, and ridge subduction propagated from northeast to southwest.

Acknowledgements

We would like to thank Professor Da-peng Zhao for the tomographic program and Professor Zhi-xin Zhao for his suggestions in regard to improving the manuscript. We also thank Associate Professor Guo-liang Zhang for providing the geochemical support. We are grateful to the two anonymous reviewers and to Professor Robert J. Stern (Editor-in-Chief) and Professor Weidong Sun (Guest Editor) for providing valuable review comments and suggestions to improve this paper.

Funding

This work is financially supported by the National Natural Science Foundation of China [grant number 40930845], [grant number 91228208]; Map Series of Geology and Geophysics of China Seas and Lands [grant number GZH200900504]; and the Strategic Priority Research Program of the Chinese Academy of Science [grant number XDA11030102].

References

Bassin, C., Laske, G., and Masters, G., 2000, The current limits of resolution for surface wave tomography in North America: EOS Transactions AGU, v. 81, p. F897.

Bautista, B.C., Bautista, M.L.C., Oike, K., Wu, F.T., and Punongbayan, R.S., 2001, A new insight on the geometry of subducting slabs in northern Luzon, Philippines: Tectonophysics, v. 339, p. 279–310. doi:10.1016/S0040-1951(01)00120-2

Bellon, H., and Yumul Jr., G.P., 2001, Miocene to Quaternary adakites and related rocks in Western Philippine arc sequences: C R Academic Sciences Paris, v. 333, p. 343–350.

Benoit, M., Aguillón-Robles, A., Calmus, T., Maury, R.C., Bellon, H., Cotten, J., Bourgois, J., and Michaud, F., 2002, Geochemical diversity of Late Miocene volcanism in southern Baja California, Mexico: Implication of mantle and crustal sources during the opening of an asthenospheric window: The Journal of Geology, v. 110, p. 627–648. doi:10.1086/342735

Besana, G.M., Negishi, H., and Ando, M., 1997, The three-dimensional attenuation structures beneath the Philippine archipelago based on seismic intensity data inversion: Earth and Planetary Science Letters, v. 151, p. 1–11. doi:10.1016/S0012-821X(97)00112-X

Bijwaard, H., Spakman, W., and Engdahl, R., 1998, Closing the gap between regional and global travel-time tomography: Journal of Geophysical Research, v. 103, p. 30055–30078. doi:10.1029/98JB02467

Cooke, D.R., Hollings, P., and Walsh, J.L., 2005, Giant porphyry deposits: Characteristics, distribution, tectonic controls: Economic Geology, v. 100, p. 801–818. doi:10.2113/gsecongeo.100.5.801

De Astis, G., Kempton, P.D., Peccerillo, A., and Wu, T.W., 2006, Trace element and isotopic variations from Mt. Vulture to Campanian volcanoes: Constraints for slab detachment and mantle inflow beneath southern Italy: Contributions to Mineralogy and Petrology, v. 151, p. 331–351. doi:10.1007/s00410-006-0062-y

Defant, M.A., and Drummond, M.S., 1990, Derivation of some modern arc magmas by melting of young subducted lithosphere: Nature, v. 347, p. 662–665. doi:10.1038/347662a0

Defant, M.J., Jacques, D., Maury, R.C., De Boer, J.D., and Joron, J.L., 1989, Geochemistry and tectonic setting of the Luzon Arc, Philippines: Geological Society of America Bulletin, v. 101, p. 663–672. doi:10.1130/0016-7606(1989)101<0663:GATSOT>2.3.CO;2

Eberhart-Phillips, D., 1986, Three-dimensional velocity structure in northern California Coast Ranges from inversion of local earthquake arrival times: Bulletin Seismol Social American, v. 76, p. 1025–1052.

Engdahl, E.R., Van der Hilst, R.D., and Buland, R., 1998, Global teleseismic earthquake relocation with improved travel times and procedures for depth determination: Bulletin Seismol Social American, v. 88, p. 722–743.

Espurt, N., Funiciello, F., Martinod, J., Guillaume, B., Regard, V., Faccenna, C., and Brusset, S., 2008, Flat subduction dynamics and deformation of the South American plate: Insights from analog modeling: Tectonics, v. 27. doi: doi:10.1029/2007TC002175

Fukao, Y., Obayashi, M., Inoue, H., and Nenbai, M., 1992, Subducting slabs stagnant in the mantle transition zone: Journal of Geophysical Research, v. 97, p. 4809–4822. doi:10.1029/91JB02749

Fukao, Y., Widiyantoro, S., and Obayashi, M., 2001, Stagnant slabs in the upper and lower mantle transition region:

Reviews of Geophysics, v. 39, p. 291–323. doi:10.1029/1999RG000068

Gasparon, M., Rosenbaum, G., Wijbrans, J., and Manetti, P., 2009, The transition from subduction arc to slab tearing: Evidence from Capraia Island, northern Tyrrhenian Sea: Journal of Geodynamics, v. 47, p. 30–38. doi:10.1016/j.jog.2008.06.004

Gutscher, M.A., Spakman, W., Bijwaard, H., and Engdahl, E.R., 2000, Geodynamics of flat subduction: Seismicity and tomographic constraints from the Andean margin: Tectonics, v. 19, p. 814–833. doi:10.1029/1999TC001152

Hamburger, M.W., Cardwell, R.K., and Isacks, B.L., 1983, Seismotectonics of the northern Philippine island arc: American Geophysical Union Monograph, v. 27, p. 1–22.

Hayes, D.E., and Lewis, S.D., 1984, A geophysical study of the Manila Trench, Luzon, Philippines: 1. Crustal structure, gravity, and regional tectonic evolution: Journal of Geophysical Research, v. 89, p. 9171–9195. doi:10.1029/JB089iB11p09171

Hsu, Y.J., Yu, S.B., Song, T.A., and Bacolcol, T., 2012, Plate coupling along the Manila subduction zone between Taiwan and northern Luzon: Journal of Asian Earth Sciences, v. 51, p. 98–108. doi:10.1016/j.jseaes.2012.01.005

Johnston, S.T., and Thorkelson, D.J., 1997, Cocos-Nazca slab window beneath Central America: Earth and Planetary Science Letters, v. 146, p. 465–474. doi:10.1016/S0012-821X(96)00242-7

Kennett, B.L.N., and Engdahl, E.R., 1991, Traveltimes for global earthquake location and phase identification: Geophysical Journal International, v. 105, p. 429–465. doi:10.1111/j.1365-246X.1991.tb06724.x

Koulakov, I., Wu, Y.M., Huang, H.H., Dobretsov, N., Jakovlev, A., Zabelina, I., Jaxybulatov, K., and Chervov, V., 2014, Slab interactions in the Taiwan region based on the P- and S-velocity distributions in the upper mantle: Journal of Asian Earth Sciences, v. 79, p. 53–64. doi:10.1016/j.jseaes.2013.09.026

Lallemand, S., Font, Y., Bijwaard, H., and Kao, H., 2001, New insights on 3D plates interaction near Taiwan from tomography and tectonic implications: Tectonophysics, v. 335, p. 229–253. doi:10.1016/S0040-1951(01)00071-3

Lévêque, J.J., Rivera, L., and Wittlinger, G., 1993, On the use of the checkerboard test to assess the resolution of tomographic inversions: Geophysical Journal International, v. 115, no. 1, p. 313–318. doi:10.1111/j.1365-246X.1993.tb05605.x

Madson, J.K., Thorkelson, D.J., Friedman, R.M., and Marshall, D.D., 2006, Cenozoic to recent plate configurations in the Pacific Basin: Ridge subduction and slab window magmatism in western North America: Geological Society of America, v. 2, p. 11–34.

Martinod, J., Funiciello, F., Faccenna, C., Labanieh, S., and Regard, V., 2005, Dynamical effects of subducting ridges: Insights from 3D laboratory models: Geophysical Journal International, v. 163, p. 1137–1150. doi:10.1111/j.1365-246X.2005.02797.x

Martinod, J., Guillaume, B., Espurt, N., Faccenna, C., Funiciello, F., and Regard, V., 2013, Effect of aseismic ridge subduction on slab geometry and overriding plate deformation: Insights from analogue modeling: Tectonophysics, v. 588, p. 39–55. doi:10.1016/j.tecto.2012.12.010

Maury, R.C., Fourcade, S., Coulon, C., Azzouzia, M.E., Bellon, H., Coutelle, A., Ouabadi, A., Semroud, B., Megartsi, M., Cotten, J., Belanteur, O., Louni-Hacini, A., Piqué, A., Capdevila, R., Hernandez, J., and Réhaulta, J., 2000, Post-collisional Neogene magmatism of the Mediterranean Maghreb margin: A consequence of slab breakoff: Comptes Rendus de l'Academie des Sciences, v. 331, p. 159–173.

Mitchell, A.G.H., Hernandez, F., and de la Cruz, A.P., 1986, Cenozoic evolution of the Philippine archipelago: Journal of Southeast Asian Earth Sciences, v. 1, p. 3–22. doi:10.1016/0743-9547(86)90003-6

Oyarzun, R., Márquez, A., Lillo, J., López, I., and Rivera, S., 2001, Giant versus small porphyry copper deposits of Cenozoic age in northern Chile: Adakitic versus normal calc-alkaline magmatism: Mineralium Deposita, v. 36, p. 794–798. doi:10.1007/s001260100205

Paige, C.C., and Saunders, M.A., 1982, LSQR: An algorithm for sparse linear equations and sparse least squares: ACM Transactions on Mathematical Software, v. 8, p. 43–71. doi:10.1145/355984.355989

Peacock, S.M., Rushmer, T., and Thompson, A.B., 1994, Partial melting of subducting oceanic crust: Earth and Planetary Science Letters, v. 121, p. 227–244. doi:10.1016/0012-821X(94)90042-6

Pe-Piper, G., and Piper, D.J., 1994, Miocene magnesian andesites and dacites, Evia, Greece: Adakites associated with subducting slab detachment and extension: Lithos, v. 31, p. 125–140. doi:10.1016/0024-4937(94)90004-3

Pilger, R.H., 1981, Plate reconstructions, aseismic ridges, and low angle subduction beneath the Andes: Geological Society of America Bulletin, v. 92, p. 448–456. doi:10.1130/0016-7606(1981)92<448:PRARAL>2.0.CO;2

Rangin, C., Le Pichon, X., Mazzotti, S., Pubellier, M., Chamot-Rooke, N., Aurelio, M., Walpersdorf, A., and Quebral, R., 1999a, Plate convergence measured by GPS across the Sundaland/Philippine Sea plate deformed boundary: The Philippines and eastern Indonesia: Geophysical Journal International, v. 139, p. 296–316. doi:10.1046/j.1365-246x.1999.00969.x

Rangin, C., Spakman, W., Pubellier, M., and Bijwaard, H., 1999b, Tomographic and geological constraints on subduction along the eastern Sundaland continental margin (South-East Asia): Bulletin De La Societe Geologique De France, v. 170, no. 6, p. 775–788.

Reay, A., and Parkinson, D., 1997, Adakites from Solander Island, New Zealand: New Zealand Journal of Geology and Geophysics, v. 40, p. 121–126.

Reich, M., Parada, M.A., Palacios, C., Dietrich, A., Schultz, F., and Lehmann, B., 2003, Adakite-like signature of Late Miocene intrusions at the Los Pelambres giant porphyry copper deposit in the Andes of central Chile: Metallogenic implications: Mineralium Deposita, v. 38, p. 876–885. doi:10.1007/s00126-003-0369-9

Rosenbaum, G., Gasparon, M., Lucente, F.P., Peccerillo, A., and Miller, M.S., 2008, Kinematics of slab tear faults during subduction segmentation and implications for Italian magmatism: Tectonics, v. 27. doi:10.1029/2007TC002143

Rosenbaum, G., and Mo, W., 2011, Tectonic and magmatic responses to the subduction of high bathymetric relief: Gondwana Research, v. 19, no. 3, p. 571–582. doi:10.1016/j.gr.2010.10.007

Russo, R.M., VanDecar, J.C., Comte, D., Mocanu, V.I., Gallego, A., and Murdie, R.E., 2010, Subduction of the Chile Ridge: Upper mantle structure and flow: GSA Today: A Publication of the Geological Society of America, v. 20, no. 9, p. 4–10. doi:10.1130/GSATG61A.1

Sajona, F.G., and Maury, R.C., 1998, Association of adakites with gold and copper mineralization in the Philippines: Comptes Rendus De L'academie Des Sciences-Series Iia-Earth Planet Sciences, v. 326, p. 27–34.

Shi, X., Qiu, X., Xia, K., and Zhou, D., 2003, Characteristics of surface heat flow in the South China Sea: Journal of Asian Earth Sciences, v. 22, p. 265–277. doi:10.1016/S1367-9120(03)00059-2

Smith, W.H.F., and Sandwell, D.T., 1997, Global seafloor topography from satellite altimetry and ship depth soundings: Science, v. 277, p. 1956–1962. doi:10.1126/science.277.5334.1956

Stephan, J.F., Blanchet, R., Rangin, C., Pelletier, B., Letouzey, J., and Muller, C., 1986, Geodynamic evolution of the Taiwan-Luzon-Mindoro belt since the late Eocene: Tectonophysics, v. 125, p. 245–268. doi:10.1016/0040-1951(86)90017-X

Suppe, J., 1988, Tectonics of arc-continent collision on both sides of the South China Sea: Taiwan and Mindoro: Acta Geological Taiwan, v. 26, p. 1–18.

Taylor, B., and Hayes, D.E., 1983, Origin and history of the South China Sea basin, *in* Hayes, D.E., ed., The tectonic and geologic evolution of Southeast Asian Seas and Islands: Part 2, Geophysical Monography Series, volume 27: Washington, DC, AGU, p. 23–56. doi:10.1029/GM027p0023.

Teng, L.S., 1990, Geotectonic evolution of Late Cenozoic arc continent collision in Taiwan: Tectonophysics, v. 183, p. 57–76. doi:10.1016/0040-1951(90)90188-E

Thorkelson, D.J., 1996, Subduction of diverging plates and the principles of slab window formation: Tectonophysics, v. 255, p. 47–63. doi:10.1016/0040-1951(95)00106-9

Thorkelson, D.J., and Breitsprecher, K., 2005, Partial melting of slab window margins: Genesis of adakitic and non-adakitic magmas: Lithos, v. 79, p. 25–41. doi:10.1016/j.lithos.2004.04.049

Thorkelson, D.J., and Taylor, R.P., 1989, Cordilleran slab windows: Geology, v. 17, p. 833–836. doi:10.1130/0091-7613(1989)017<0833:CSW>2.3.CO;2

Um, J., and Thurber, C.H., 1987, A fast algorithm for two-point seismic ray tracing: Bulletin of the Seismological Society of America, v. 77, no. 3, p. 972–986.

Van Hunen, J., van den Berg, A.P., and Vlaar, N.J., 2002, On the role of subducting oceanic plateaus in the development of shallow flat subduction: Tectonophysics, v. 352, p. 317–333. doi:10.1016/S0040-1951(02)00263-9

Widiyantoro, S., and Van der Hilst, R.D., 1997, Mantle structure beneath Indonesia inferred from high resolution tomographic imaging: Geophysical Journal International, v. 130, p. 167–182. doi:10.1111/j.1365-246X.1997.tb00996.x

Wright, C., 2009, The P wavespeed structure in the mantle to 800 km depth below the Philippines region: Geodynamic implications: Tectonophysics, v. 466, p. 152–161. doi:10.1016/j.tecto.2007.11.001

Wright, C., and Kuo, B., 2007, Evidence for an elevated 410 km discontinuity below the Luzon, Philippines region and transition zone properties using seismic stations in Taiwan and earthquake sources to the south: Earth Planets and Space, v. 59, no. 6, p. 523–539.

Yang, T.F., Lee, T., Chen, C.H., Cheng, S.N., Knittel, U., Punongbayan, R.S., and Rasdas, A.R., 1996, A double island arc between Taiwan and Luzon: Consequence of ridge subduction: Tectonophysics, v. 258, p. 85–101. doi:10.1016/0040-1951(95)00180-8

Yogodzinski, G.M., Lees, J.M., Churikova, T.G., Dorendorf, F., Wöerner, G., and Volynets, O.N., 2001, Geochemical evidence for the melting of subducting oceanic lithosphere at plate edges: Nature, v. 409, p. 500–504. doi:10.1038/35054039

Yumul Jr., G.P., Dimalanta, C.B., Bellon, H., Faustino, D.V., De Jesus, J.V., Tamayo Jr., R.A., and Jumawan, F.T., 2000, Adakitic lavas in the Central Luzon back-arc region, Philippines: Lower crust partial melting products?: The Island Arc, v. 9, p. 499–512. doi:10.1046/j.1440-1738.2000.00297.x

Yumul Jr., G.P., Dimalanta, C.B., Maglambayan, V.B., and Marquez, E.J., 2008, Tectonic setting of a composite terrane: A review of the Philippine Island arc system: Geosciences Journal, v. 12, p. 7–17. doi:10.1007/s12303-008-0002-0

Zandt, G., and Humphreys, E., 2008, Toroidal mantle flow through the western U.S. slab window: Geology, v. 36, p. 295–298. doi:10.1130/G24611A.1.

Zhao, D., Hasegawa, A., and Kanamori, H., 1994, Deep structure of Japan subduction zone as derived from local, regional, and teleseismic events: Journal of Geophysical Research, v. 99, p. 22313–22329. doi:10.1029/94JB01149

Zhao, D., Yamamoto, Y., and Yanada, T., 2013, Global mantle heterogeneity and its influence on teleseismic regional tomography: Gondwana Research, v. 23, p. 595–616. doi:10.1016/j.gr.2012.08.004

Zhao, D.P., Hasegawa, A., and Horiuchi, S., 1992, Tomographic imaging of P and S wave velocity structure beneath northeastern Japan: Journal of Geophysical Research, v. 97, p. 19909–19928. doi:10.1029/92JB00603